

## ARTICLE

## Electron Momentum Spectroscopy Study on Inner Orbitals of Methyl iodide

Min-fu Zhao<sup>a, b</sup>, Shan-shan Niu<sup>a</sup>, Qi-guo Tian<sup>a</sup>, Jing Yang, Xu Shan<sup>a\*</sup>, Xiang-jun Chen<sup>a</sup>*a.* Hefei National Laboratory for Physical Sciences at the Microscale and Department of Modern Physics, University of Science and Technology of China, Hefei 230026, China*b.* Department of Experiment and Practical Training Management, Research Center of Atoms and Molecules and Optical Applications, West Anhui University, Lu'an 237012, China

(Dated: Received on October 2, 2020; Accepted on November 8, 2020)

The binding energy spectrum and electron momentum profiles of the inner orbitals of methyl iodide have been measured using an electron momentum spectrometer at the impact energy of 1200 eV plus binding energy. Two peaks in the binding energy spectrum, arising from the spin-orbit splitting, are observed and the corresponding electron momentum profiles are obtained. Relativistic density functional calculations are performed to elucidate the experimental electron momentum profiles of two spin-orbit splitting components, showing agreement with each other except for the intensity in low momentum region. The measured high intensity in the low momentum region can be further explained by the distorted wave calculation.

**Key words:** Electron momentum spectroscopy, Relativistic effect, Spin-orbit coupling, Distorted wave effect

## I. INTRODUCTION

In atoms or molecules, especially for those containing high- $Z$  elements, the relativistic effect is noticeable, not only causing the energy of electronic states to shift or split, but also affecting the electronic wavefunctions, which plays a vital role in understanding the physical and chemical properties of matter [1–3]. Photoelectron spectroscopy (PES) is the most widely used experimental technique to study the relativistic effect by measuring the spin-orbit (SO) splitting energy and the branching ratio for SO splitting components as a function of photon energy [4–8]. Electron momentum spectroscopy (EMS) [9–11] provides an alternative experimental method to directly evaluate the relativistic effect on the electronic wavefunctions of atoms and molecules due to its unique ability in measuring the electron momentum profile (EMP) of individual orbitals. In the pioneer work of Cook *et al.* [12, 13], they observed the influence of the relativistic effect on the electronic wavefunctions of two SO splitting components,  $5p_{3/2}$  and  $5p_{1/2}$ , from Xe  $5p$  electron ionization. The similar results were achieved for  $6p_{3/2}$  and  $6p_{1/2}$  doublet of lead by Frost *et al.* [14]. For inner shell  $4d$  orbital of xenon, the relativistic effects on the EMPs for the SO components  $4d_{3/2}$  and  $4d_{5/2}$  were investigated by Ren *et al.* at different electron collision energies [15]. For molecular systems, Li *et al.* [16] reported the rela-

tivistic effect on the highest occupied molecular orbital (HOMO) of  $\text{CF}_3\text{I}$  for the first time. Subsequently, Ning and co-workers reported the relativistic EMS studies for  $\text{I}_2$  molecule [17, 18] and Wang *et al.* discussed the relativistic effect on the HOMO of  $n$ -propyl iodide [19]. Recently, Niu *et al.* [20] presented the detailed EMS study on the valence orbitals of methyl iodide ( $\text{CH}_3\text{I}$ ), in which the relativistic effects were revealed not only for the SO components ( $2e_{3/2}$  and  $2e_{1/2}$ ) and the C–I bonding orbital ( $3a_1$ ), but also for the inner valence orbitals ( $2a_1$ ). However, relativistic EMS studies for the inner or core orbitals of atoms and molecules are very scarce. The main difficulty or obstacle may lie in two aspects: one is the extremely low cross sections of electron-impact ionization for inner orbitals and the other is the complexities for theoretical treatments.

In this work, we report an EMS experiment on the inner orbitals of  $\text{CH}_3\text{I}$  using a high-sensitivity EMS spectrometer [21]. The experimental EMPs of two SO splitting components are obtained. For comparison, the calculations have been performed by using the relativistic density functional theory [22, 23] and the distorted wave approximation method [24].

## II. EXPERIMENTAL AND THEORETICAL BACKGROUND

EMS is based on an electron-impact-induced single ionization process, also called  $(e, 2e)$  reaction, in which the incident electron with a certain energy (typically 1200 eV) collides with atomic or molecular targets and is scattered, and an electron is knocked out in the single

\* Author to whom correspondence should be addressed. E-mail: xshan@ustc.edu.cn

ionization of the target. The conservation of energy and momentum enable us to derive the binding energy  $\varepsilon$  and the momentum  $\mathbf{p}$  of the target orbital electron as

$$\varepsilon = E_0 - E_1 - E_2 \quad (1)$$

$$\mathbf{p} = \mathbf{p}_1 + \mathbf{p}_2 - \mathbf{p}_0 \quad (2)$$

where  $E_0$ ,  $E_1$  and  $E_2$  are energies, and  $\mathbf{p}_0$ ,  $\mathbf{p}_1$  and  $\mathbf{p}_2$  are momenta for the incident, scattered and ejected electrons, respectively.

In EMS experiments, non-coplanar symmetric kinematics arrangement is mostly employed where the energies and polar angles of two outgoing electrons are equal ( $E_1=E_2$ ,  $\theta_1=\theta_2=\theta=45^\circ$ ) and the relative azimuthal angle between two outgoing electrons,  $\phi=\pi-(\phi_2-\phi_1)$ , is varied. Under these conditions the magnitude of target electron momentum is given by

$$p = \sqrt{(p_0 - 2p_1 \cos \theta)^2 + [2p_1 \sin \theta \sin(\phi/2)]^2} \quad (3)$$

A detailed description of the spectrometer used in the CH<sub>3</sub>I experiment can be found in Ref.[21]. Here only a brief introduction is presented. The incident electron beam generated by an electron gun is accelerated by a lens system to the desired energy of 1200 eV plus the binding energy and transferred to the reaction region where the incident electron impacts with the gas-phase target molecule injected by a nozzle. The scattered and ejected electrons with  $\sim 600$  eV energies outgoing from the reaction region along  $45^\circ$  polar angle enter into the five-element conical lens to retard their energies being 200 eV, then pass through a  $90^\circ$  sector,  $2\pi$  spherical electrostatic analyzer to disperse different exit positions, and immediately are detected in coincidence by a position sensitive detector placed at the exit plane of the analyzer. Before CH<sub>3</sub>I experiments, the instrumental energy and momentum resolutions were calibrated to be  $\sim 1.5$  eV and  $\sim 0.20$  a.u., respectively, by measuring the ionization energy spectrum and the EMP of Ar 3p orbital.

For the theoretical treatment, under a series of approximations including the binary encounter, the weak-coupling, the plane wave impulse approximations (PWIA), and the target Hartree-Fock approximation or Kohn-Sham approximation, the triple differential cross section (TDCS) of EMS can be expressed as [9, 25]:

$$\sigma_{\text{EMS}} \propto \frac{1}{4\pi} \int |\varphi_i(\mathbf{p})|^2 d\Omega \quad (4)$$

where  $\varphi_i(\mathbf{p})$  represents the canonical Hartree-Fock (HF) or Kohn-Sham (KS) orbital. It can be seen from the Eq.(4) that EMS measurement is directly linked with the spherically averaged modulus square of the orbital wavefunction in momentum space, *i.e.*, electron momentum profile.

For the case of CH<sub>3</sub>I molecule containing heavy element, the theoretical calculations should take the relativistic effect into account. However, four-component

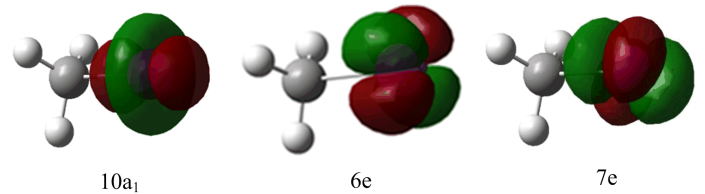


FIG. 1 Orbital maps of 10a<sub>1</sub>, 6e, and 7e of CH<sub>3</sub>I calculated by B3LYP/aug-cc-pVTZ-PP.

all-electron relativistic calculations for molecules are still difficult. Relativistic pseudo-potential basis sets employed usually presents an alternative approach [16, 20], but invalid for spin-orbit coupling effects. Recently, Amsterdam density functional method (ADF) [22, 23] was introduced to the EMS studies [17–20], which can calculate two-component (SO coupling) and scalar relativistic wavefunctions. The orbital wavefunction in position space generated by SO coupling relativistic method in ADF program can be described as

$$\varphi_i(\mathbf{r}) = \varphi_\alpha(\mathbf{r})\alpha + \varphi_\beta(\mathbf{r})\beta \quad (5)$$

where  $\alpha$  and  $\beta$  are the spin variables which are orthogonal with each other, and  $\varphi_\alpha(\mathbf{r})$  and  $\varphi_\beta(\mathbf{r})$  are the relevant position space wavefunctions. Then, through Fourier transform, the cross section of EMS can be given by

$$\sigma_{\text{EMS}} \propto \frac{1}{4\pi} \int (|\varphi_\alpha(\mathbf{p})|^2 + |\varphi_\beta(\mathbf{p})|^2) d\Omega \quad (6)$$

where  $\varphi_\alpha(\mathbf{p})$  and  $\varphi_\beta(\mathbf{p})$  are the momentum space electron wave-functions for the spin  $\alpha$  and  $\beta$  components.

In the present calculations, molecular geometry of CH<sub>3</sub>I on the ground state is optimized by Gaussian 09 program [26] using the nonrelativistic B3LYP method and aug-cc-pVTZ-PP basis set which includes small-core energy-consistent relativistic pseudo-potentials (PP) for I [27] and augmented correlation consistent polarized valence triple-zeta basis functions for C and H. The ground state electronic configuration and the corresponding orbital maps are calculated at the same theoretical level. For the relativistic calculations, two-component orbital wavefunctions in position space are obtained by the ADF program [22, 23] using the relativistic B3LYP functional method and the quadruple zeta basis sets with four polarization functions (QZ4P). According to the Eqs. (5) and (6), the theoretical EMPs for two SO components are achieved.

### III. RESULTS AND DISCUSSION

CH<sub>3</sub>I molecule including 62 electrons belongs to C<sub>3v</sub> point group, and its ground state electronic configura-

tion can be written as:

$$\begin{array}{l}
 \underbrace{(1a_1)^2(2a_1)^2(3a_1)^2(1e)^4(4a_1)^2(5a_1)^2(2e)^4(6a_1)^2}_{\text{core}} \\
 \underbrace{(8a_1)^2(9a_1)^2(5e)^4(10a_1)^2(6e)^4(7e)^4}_{\text{inner orbitals}} \\
 \underbrace{(11a_1)^2(12a_1)^2(8e)^4(13a_1)^2(9e)^4}_{\text{valence orbitals}}
 \end{array} \quad (7)$$

The above orbital sequence is referred from the calculation of B3LYP/aug-cc-pVTZ-PP. Since the valence orbitals of CH<sub>3</sub>I have been studied in detail by Niu *et al.* [20], in this work, we focus on the inner orbitals 10a<sub>1</sub>, 6e and 7e. Their orbital maps in position space are calculated by B3LYP/aug-cc-pVTZ-PP, as shown in FIG. 1, indicating that they are essentially iodine atomic 4d lone pair orbitals. These three orbitals will energetically degenerate and can be approximated as one.

The ionization energy spectra for 10a<sub>1</sub>, 6e, and 7e inner orbitals of CH<sub>3</sub>I have been extensively investigated by photoelectron spectroscopy experiments [28–31]. Due to the SO coupling effect, the ionic state from their ionizations is split into two components (hereafter SO-1 and SO-2, also noted as d<sub>5/2</sub> and d<sub>3/2</sub> in the literatures [28–31]) whose energies were determined by the photoelectron spectroscopy to be about 56.7 eV and 58.3 eV, respectively.

FIG. 2 shows the binding energy spectrum (BES) measured by present EMS experiment for 10a<sub>1</sub>, 6e, and 7e inner orbitals of CH<sub>3</sub>I. It can be seen that two SO splitting components are observed clearly, very similar to the structural features of photoelectron spectroscopy experiments [28–31]. In order to extract experimental EMPs for individual SO components, two Gaussian peaks are used to fit the BES at different azimuthal angles. The peak positions of these Gaussian functions are referred to the high-resolution photoelectron spectroscopy results [28]. The peak widths represent our instrumental energy resolution together with the Franck-Condon widths from the ionizations.

The experimental EMPs for 10a<sub>1</sub>, 6e, and 7e inner orbitals, as well as for two SO splitting components (SO-1 and SO-2) are shown in FIG.3, FIG.4 and FIG.5, respectively. The error bars of experimental data include the uncertainties from the statistics and deconvolution processes. For comparison, the theoretical EMPs calculated by the two-component relativistic B3LYP/QZ4P are also shown in the figures. The theoretical EMPs are folded with the instrumental momentum resolution (angular resolution:  $\Delta\theta\approx 1.0^\circ$ ,  $\Delta\phi\approx 3.0^\circ$ ) using the Gaussian weighted planar grid method [32]. In addition, the experimental and calculated EMPs are placed on a common intensity scale by normalizing the experimental EMP for these three orbitals to the corresponding theoretical one in the momentum range from 1.0 a.u. to 3.5 a.u.

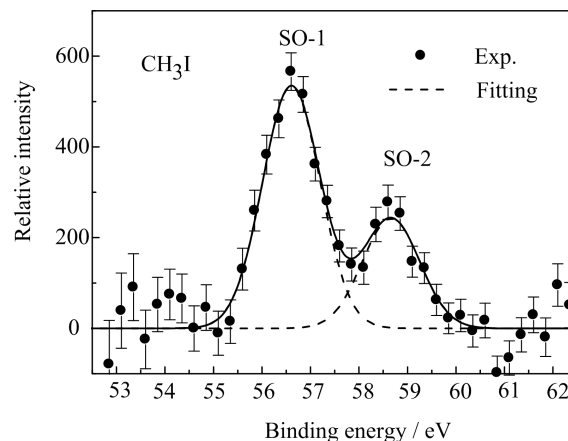


FIG. 2 The binding energy spectrum of 10a<sub>1</sub>, 6e, and 7e inner orbitals of CH<sub>3</sub>I. The dash lines represent two Gaussian peaks used to fit the BES, and the solid line is their sum.

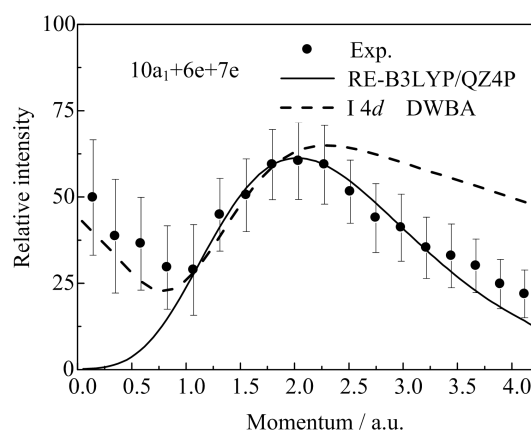


FIG. 3 Experimental and theoretical EMPs for 10a<sub>1</sub>, 6e and 7e inner orbitals of CH<sub>3</sub>I. The solid line represents the relativistic B3LYP/QZ4P calculation for molecular orbitals while the dash line is the distorted wave calculation for atomic I 4d orbital.

FIG. 3 presents the experimental and theoretical EMPs of 10a<sub>1</sub>, 6e and 7e orbitals of CH<sub>3</sub>I. The calculation predicts a p-type momentum profile with a maximum at the momentum  $p\approx 2.0$  a.u. agreeing with the measurement except for the intensity in the low momentum region of  $p<1.0$  a.u. The similar high intensities at the low momentum have been also observed in previous studies for atomic d orbitals or molecular  $\pi^*$ -like orbitals [33–36], which were ascribed to the distorted wave effects. However, for molecular systems, it is difficult to accomplish the distorted wave calculations due to the multi-center feature of molecules. In the present case, 10a<sub>1</sub>, 6e and 7e orbitals of CH<sub>3</sub>I are primarily consisted of atomic I 4d lone pair orbital. Therefore the calculation for I 4d orbital is performed by the distorted wave approximation method of McCarthy which is widely used to calculate the ionization cross sections for atomic systems [24]. Under this approximation, the

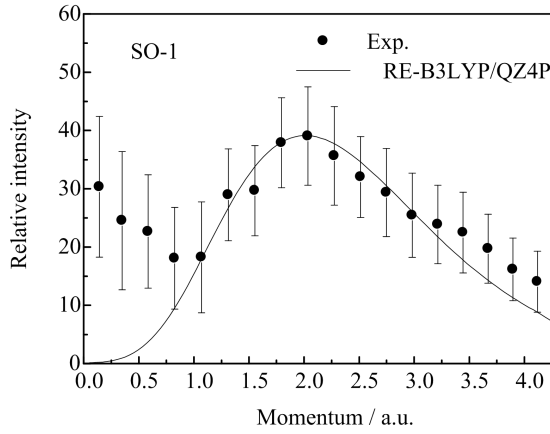


FIG. 4 Experimental and theoretical EMPs for the SO-1 component for  $10a_1$ ,  $6e$ , and  $7e$  orbitals of  $\text{CH}_3\text{I}$ .

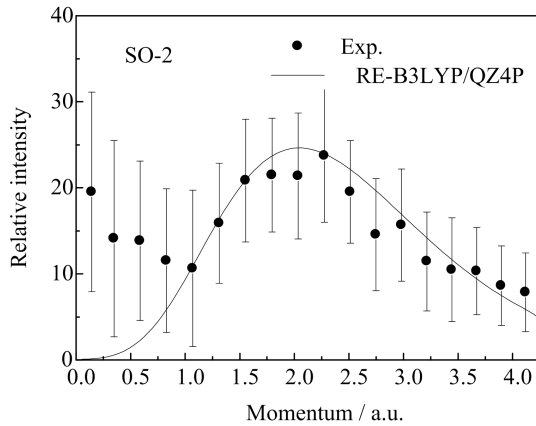


FIG. 5 Experimental and theoretical EMPs for the SO-2 component of  $10a_1$ ,  $6e$  and  $7e$  orbitals of  $\text{CH}_3\text{I}$ .

TDCS is written as

$$\frac{d^3\sigma}{d\Omega_1 d\Omega_2 dE_1} = (2\pi)^4 \frac{p_1 p_2}{p_0} \sum_{av} (|f|^2 + |g|^2 - \text{Re}(f^*g)) \quad (8)$$

$$f \equiv \langle \chi^{(-)}(\mathbf{p}_1, \mathbf{r}_1) \chi^{(-)}(\mathbf{p}_2, \mathbf{r}_2) | V_{12} | \chi^{(+)}(\mathbf{p}_0, \mathbf{r}_1) \psi_{nl} \rangle \quad (9)$$

$$g \equiv \langle \chi^{(-)}(\mathbf{p}_1, \mathbf{r}_2) \chi^{(-)}(\mathbf{p}_2, \mathbf{r}_1) | V_{12} | \chi^{(+)}(\mathbf{p}_0, \mathbf{r}_1) \psi_{nl} \rangle \quad (10)$$

where  $\sum$  represents the sum over final and average over initial magnetic and spin degeneracy.  $\mathbf{r}_1$  and  $\mathbf{r}_2$  are the coordinates of two outgoing electrons.  $V_{12}=1/|\mathbf{r}_1 - \mathbf{r}_2|$  is the interaction potential between the incident and target electrons responsible for the ionization.  $\psi_{nl}$  represents the  $nl$  orbital of the target.  $\chi^{(+)}$  is the distorted wavefunction for the incident electron generated in the equivalent local ground state potential of the initial state, and  $\chi^{(-)}$  denotes the distorted wavefunctions for two outgoing electrons generated in the equivalent local ground state potential of the final state. The detailed description about theoretical calculations has been presented in Ref.[24].

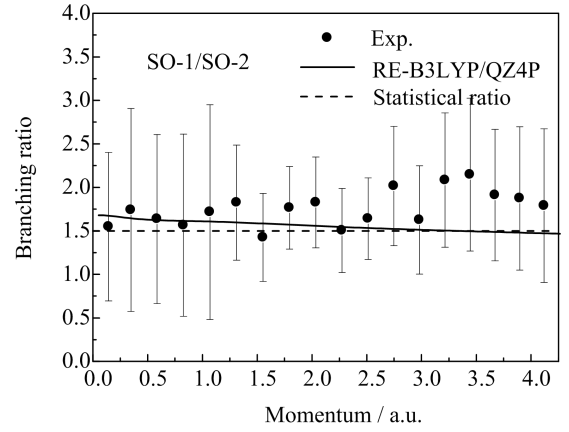


FIG. 6 The branching ratio of the EMPs for SO-1 and SO-2 components. The solid line represents the result of relativistic B3LYP/QZ4P calculations while the dashed line is the statistical ratio.

As shown in FIG. 3, a good accordance is found between the experiment and the distorted wave calculation at the low momentum region, indicating the result of the distorted wave effect on the inner orbitals of  $\text{CH}_3\text{I}$ .

FIG. 4 and FIG. 5 show the experimental and theoretical EMPs for SO-1 and SO-2, respectively. It is noted that the two-component relativistic B3LYP/QZ4P calculation is under the PWIA approximation. Here the distorted wave effect cannot be taken into account. It can be seen from the figures that the experimental and theoretical EMPs of SO-1 and SO-2 components display a good agreement with each other except for the intensities at  $p < 1.0$  a.u.

FIG. 6 shows the branching ratios of SO-1 and SO-2. The difference between the momentum profiles of SO-1 and SO-2 can be clearly seen from the figure. The dashed line represents the statistical ratio of 3:2 while the prediction of relativistic calculations obviously deviates from the value of 3:2 as the solid line shown in FIG. 6 which is the result of relativistic effects on the wavefunctions for different SO components. For the experimental data, though the intensity ratio of the measured EMPs for SO-1 and SO-2 is generally consistent with the theoretical predictions, it is very hard to directly judge the difference of relativistic effects on the wavefunctions for two SO components. Similar phenomena were also observed for two SO components,  $4d_{5/2}$  and  $4d_{3/2}$ , from the ionization of atomic Xe 4d inner-shell orbitals [15]. Some possible reasons may result in the difficulty of observing the SO coupling effect on the inner orbitals from EMS experiments. One is the distorted wave effect and the multi-electron effect which maybe contaminate the SO effect on the wavefunctions. Another is very low cross sections of electron impact ionization for the inner orbitals which maybe bring out large error bars of the experimental data.

#### IV. CONCLUSION

The EMS study on the binding energy spectrum and electron momentum profiles for two SO splitting components arising from the ionization of  $10a_1$ ,  $6e$  and  $7e$  inner orbitals of methyl iodide have been reported for the first time. Relativistic density functional calculations are carried out to elucidate the experimental EMPs of these two components, showing agreement except for the intensity in low momentum region which is explained by the distorted wave calculation. The present study indicates that the relativistic effect plays a noticeable role in ionization energy splitting and wavefunctions for the inner orbitals of molecules.

#### V. ACKNOWLEDGMENTS

This work was supported by the National Natural Science Foundation of China (No.11534011 and No.11874339) and the Natural Science Research Programme of Education Department of Anhui Province (No.KJ2013A260 and No.KJ2016A749).

- [1] K. S. Pitzer, *Acc. Chem. Res.* **12**, 271 (1979).
- [2] P. Pyykko and J. P. Desclaux, *Acc. Chem. Res.* **12**, 276 (1979).
- [3] P. Pyykko, *Chem. Rev.* **88**, 563 (1988).
- [4] B. W. Yates, K. H. Tan, L. L. Coatsworth, and G. M. Bancroft, *Phys. Rev. A* **31**, 1529 (1985).
- [5] S. Aksela, K. H. Tan, G. M. Bancroft, H. Aksela, B. W. Yates, and L. L. Coatsworth, *Phys. Rev. A* **32**, 1219 (1985).
- [6] S. M. Huttula, S. Heinäsmäki, S. Fritzsche, H. Aksela, E. Kukk, M. Huttula, and S. Aksela, *J. Electron. Spectrosc. Rel. Phenom.* **150**, 35 (2006).
- [7] M. O. Krause, T. A. Carlson, and P. R. Woodruff, *Phys. Rev. A* **24**, 1374 (1981).
- [8] T. A. Carlson, A. Fahlman, M. O. Krause, P. R. Keller, J. W. Taylor, T. Whitley, and F. A. Grimm, *J. Chem. Phys.* **80**, 3521 (1984).
- [9] I. E. McCarthy and E. Weigold, *Rep. Prog. Phys.* **54**, 789 (1991).
- [10] C. E. Brion, *Int. J. Quantum Chem.* **29**, 1397 (1986).
- [11] M. A. Coplan, J. H. Moore, and J. P. Doering, *Rev. Mod. Phys.* **66**, 985 (1994).
- [12] J. P. D. Cook, J. Mitroy, and E. Weigold, *Phys. Rev. Lett.* **52**, 1116 (1984).
- [13] J. P. D. Cook, I. E. McCarthy, J. Mitroy, and E. Weigold, *Phys. Rev. A* **33**, 211 (1986).
- [14] L. Frost, J. Mitroy, and E. Weigold, *J. Phys. B: At. Mol. Phys.* **19**, 4063 (1986).
- [15] X. G. Ren, C. G. Ning, J. K. Deng, G. L. Su, S. F. Zhang, and Y. R. Huang, *Phys. Rev. A* **73**, 042714 (2006).
- [16] Z. J. Li, X. J. Chen, X. Shan, X. X. Xue, T. Liu, and K. Z. Xu, *Chem. Phys. Lett.* **457**, 45 (2008).
- [17] K. Liu, C. G. Ning, and J. K. Deng, *Phys. Rev. A* **80**, 022716 (2009).
- [18] J. S. Zhu, J. K. Deng, and C. G. Ning, *Phys. Rev. A* **85**, 052714 (2012).
- [19] E. L. Wang, Y. F. Shi, X. Shan, H. J. Yang, W. Zhang, and X. J. Chen, *Chin. J. Chem. Phys.* **27**, 503 (2014).
- [20] S. S. Niu, Y. Tang, Z. H. Liu, Y. F. Shi, E. L. Wang, X. Shan, and X. J. Chen, *Phys. Rev. A* **99**, 022512 (2019).
- [21] Q. G. Tian, K. D. Wang, X. Shan, and X. J. Chen, *Rev. Sci. Instrum.* **82**, 033110 (2011).
- [22] G. t. Te Velde, F. M. Bickelhaupt, E. J. Baerends, C. Fonseca Guerra, S. J. van Gisbergen, J. G. Snijders, and T. Ziegler, *J. Comput. Chem.* **22**, 931 (2001).
- [23] C. F. Guerra, J. Snijders, G. t. Te Velde, and E. Baerends, *Theor. Chem. Acc.* **99**, 391 (1998).
- [24] I. E. McCarthy, *Aust. J. Phys.* **48**, 1 (1995).
- [25] P. Duffy, D. P. Chong, M. E. Casida, and D. R. Salahub, *Phys. Rev. A* **50**, 4707 (1994).
- [26] M. J. Frisch, G. W. Trucks, H. B. Schlegel, G. E. Scuseria, M. A. Robb, J. R. Cheeseman, G. Scalmani, V. Barone, B. Mennucci, G. A. Petersson, H. Nakatsuji, M. Caricato, X. Li, H. P. Hratchian, A. F. Izmaylov, J. Bloino, G. Zheng, J. L. Sonnenberg, M. Hada, M. Ehara, K. Toyota, R. Fukuda, J. Hasegawa, M. Ishida, T. Nakajima, Y. Honda, O. Kitao, H. Nakai, T. Vreven, J. A. Jr. Montgomery, J. E. Peralta, F. Ogliaro, M. Bearpark, J. J. Heyd, E. Brothers, K. N. Kudin, V. N. Staroverov, R. Kobayashi, J. Normand, K. Raghavachari, A. Rendell, J. C. Burant, S. S. Iyengar, J. Tomasi, M. Cossi, N. Rega, N. J. Millam, M. Klene, J. E. Knox, J. B. Cross, V. Bakken, C. Adamo, J. Jaramillo, R. Gomperts, R. E. Stratmann, O. Yazyev, A. J. Austin, R. Cammi, C. Pomelli, J. W. Ochterski, R. L. Martin, K. Morokuma, V. G. Zakrzewski, G. A. Voth, P. Salvador, J. J. Dannenberg, S. Dapprich, A. D. Daniels, Ö. Farkas, J. B. Foresman, J. V. Ortiz, J. Cioslowski, and D. J. Fox, *Gaussian 09, Revision A02*, Wallingford, CT: Gaussian Inc., (2009).
- [27] K. A. Peterson, B. C. Shepler, D. Figgen, and H. Stoll, *J. Phys. Chem. A* **110**, 13877 (2006).
- [28] D. M. P. Holland, I. Powis, G. Öhrwall, L. Karlsson, and W. von Niessen, *Chem. Phys.* **326**, 535 (2006).
- [29] J. N. Cutler, G. M. Bancroft, and K. H. Tan, *J. Chem. Phys.* **97**, 7932 (1992).
- [30] G. O'Sullivan, *J. Phys. B: At. Mol. Phys.* **15**, L327 (1982).
- [31] D. W. Lindle, P. H. Kobrin, C. M. Truesdale, T. A. Ferrett, P. A. Heimann, H. G. Kerckhoff, U. Becker, and D. A. Shirley, *Phys. Rev. A* **30**, 239 (1984).
- [32] P. Duffy, M. E. Casida, C. E. Brion, and D. P. Chong, *Chem. Phys.* **159**, 347 (1992).
- [33] C. E. Brion, Y. Zheng, J. Rolke, J. J. Neville, I. E. McCarthy, and J. Wang, *J. Phys. B: At. Mol. Opt. Phys.* **31**, L223 (1998).
- [34] X. G. Ren, C. G. Ning, J. K. Deng, S. F. Zhang, G. L. Su, F. Huang, and G. Q. Li, *Phys. Rev. Lett.* **94**, 163201 (2005).
- [35] C. G. Ning, X. G. Ren, J. K. Deng, G. L. Su, S. F. Zhang, and G. Q. Li, *Phys. Rev. A* **73**, 022704 (2006).
- [36] Y. Miyake, M. Takahashi, N. Watanabe, Y. Khajuria, Y. Udagawa, Y. Sakai, and T. Mukoyama, *Phys. Chem. Chem. Phys.* **8**, 3022 (2006).